E3S Web of Conferences **12**, 02002 (2016) DOI: 10.1051/e3sconf/20161202002
i-DUST 2016

Polarisation properties of [SQUID]^2 horizontal components at the LSBB (*Laboratoire Souterrain à Bas Bruit*)

Christian Kwisanga[a]

Department of Physics, College of Science and Technology, University of Rwanda, Rwanda

Abstract. Polarisation properties of the geomagnetic signal are computed using the coherence matrix of horizontal components (EW and NS) of the [SQUID]^2 datasets, in a relatively small bandwidth. Wavefront ellipticity, signal-to-noise ratio (*snr*) and wavefront arrival angle of the magnetic quasi-monochromatic waves are determined. From the variation of ellipticity extremum position in the vicinity of 8 Hz, the temporal variation of the peak frequency is traced for the LSBB and two Northern American stations distant from the LSBB by $\sim$8,000 km. The spectra of the peak frequency variation display the daily, half daily and third-daily harmonics at all stations, which are characteristic of the first Schumann resonance. Ellipticity spectrograms also unveil a type of chirping local nighttime resonances, known as ionospheric Alfvén resonances (IAR), observed at all stations. Thanks to the *snr* spectrograms, components of the signal which are local to the LSBB station are cancelled from the output, particularly the 50-Hz power grid signal which is minimised in the *snr* spectra.

1. Introduction

At the extremely low frequency (ELF [3−3000 Hz]) range, the main source of natural electromagnetic energy in the Earth-ionospheric cavity is due to thunderstorm activity and the cavity that acts as a resonator for specific modes called Schumann resonances (SR) [1]. The sources of electromagnetic pulse excitation is random in time and space around the globe, with hotspots in continental tropical areas. The interference between electromagnetic pulses generated worldwide forms SR with eigenfrequencies at 7.8, 14, 20 Hz [2]. The random nature of generation and phase distribution of pulses form at a ground station a superposition of fully polarised and depolarised waves [1].

The polarisation study of geomagnetic components in the ELF range is an important tool to assess whether electromagnetic SR measured at an observatory are of global nature. Coherence is the measure of the degree of polarisation of electromagnetic waves. It has two aspects: Spatial and temporal coherence. Spatial coherence determines the correlation between waves at different points in space and temporal coherence defines their correlation between wavefronts at different instants in time. Here, time coherence is evaluated by determining the rate of variation of the amplitude and phase of the electromagnetic wavefront. Polarisation properties of the magnetic wave are computed using quasi-monochromatic wave theory in the frequency domain [3]. The method is based on the auto-correlation and cross-correlation of components of the power wavefield called the coherence matrix (CM).

[a] e-mail: kwistiand@gmail.com

In this paper, we attempt to establish a correlation between magnetic datasets measured at the LSBB using the Superconductive Quantum Interference Device Qualified for Ionospheric Detection ([SQUID]^2) and the Canadian Array for Realtime Investigations of Magnetic Activity (CARISMA) network using the high permittivity Induction Coil Magnetometers (ICM).

2. Computation of polarisation properties

The non-polarised and polarised components of the horizontal geomagnetic field (H) can be resolved by computing eigenvalues and eigenvectors of the CM, considering H components as quasi-monochromatic waves [3]. The two components are

$$H_X = A_1(t)\ \exp[i(\bar{\omega}t + \varphi_1(t))] \tag{1}$$

$$H_Y = A_2(t)\ \exp[i(\bar{\omega}t + \varphi_2(t))] \tag{2}$$

where $\bar{\omega} = 2\pi\bar{\upsilon}$ is the average angular frequency of the wave packet, $A_1(t)$, $A_2(t)$ respective time-dependent amplitudes and $\varphi_1(t)$, $\varphi_2(t)$ are time-varying phases.

2.1 Coherence

The polarisation of the wavefield can be represented as the coherence matrix (CM) of the form

$$J = \begin{bmatrix} J_{XX} & J_{XY} \\ J_{YX} & J_{YY} \end{bmatrix} = \begin{bmatrix} < H_X H_X^* > & < H_X H_Y^* > \\ < H_Y H_X^* > & < H_Y H_Y^* > \end{bmatrix} \tag{3}$$

where H_X^*, H_Y^* are complex conjugates to the horizontal magnetic waves. In case the wave is fully polarised, then $\det(J) = 0$. The intensity of the total wave packet would be obtained by plugging (1) and (2) into (3)

$$I = J_{XX} + J_{YY} = A_1^2 + A_2^2. \tag{4}$$

In case the signal is not fully polarised, $\det(J) \neq 0$. The degree of polarisation of the wave is the ratio of the polarised to the total wave intensity. By solving eigenvalues of (3), the degree of polarisation (coherence) can hence be expressed as

$$P_D = \left[1 - \frac{4|J|}{(J_{XX} + J_{YY})^2}\right]^{\frac{1}{2}}. \tag{5}$$

P_D is always positive and varies from 0 to 1. $P_D = 0$ represents a completely depolarised signal and $P_D = 1$ a totally polarised signal.

2.2 Ellipticity

Ellipticity is a property that determines the type and the direction of rotation of the polarised electromagnetic wave in time. Elliptical polarisation properties are obtained from the CM as follows [4]

$$\frac{Y^2}{P_{YY}} + \frac{2RePXY}{P_{XX}P_{YY}} + \frac{X^2}{P_{XX}} = 1. \tag{6}$$

Equation (6) is a typical equation of an ellipse. Parameters associated with the ellipse are depicted in Fig. 1: The direction of polarisation β and the angle of inclination of the ellipse θ.

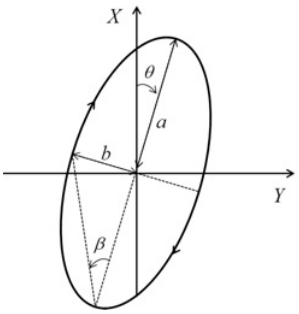

Figure 1. Sketch of the elliptical polarisation of the horizontal H, where a, b represent the semi-major and semi-minor axes of the ellipse. Axes x and y represent the WE and SN directions. θ represents the inclination angle of the major axis of the ellipse to the X axis. The direction of polarisation represented here is right handed in the direction of z [5].

β can be deduced from (6) as $\sin 2\beta = \left[i(P^*_{XY} - P_{XY})\right]\left[(P_{XX} - P_{YY})^2 + 4P^*_{XY}P_{XY}\right]^{-\frac{1}{2}}$. Ellipticity is hence

$$el = \tan\,\beta = \frac{b}{a}\cdot \tag{7}$$

By convention, when the angle $\beta < 0$ ($el < 0$), the polarisation is clockwise or right-handed as shown in Fig. 1, and $\beta > 0$ ($el > 0$), the polarisation is counter-clockwise or left-handed. The value of ellipticity varies as $|el| \leq 1$, with $el = 0$ describing linear polarisation and $|el| = 1$ circular polarisation.

2.3 Inclination angle of the polarisation ellipse

The inclination angle is the angle made between the semi-major axis and the X axis as shown in Fig. 1. The relationship between the inclination of the ellipse and the coherence matrix is [4]

$$\tan 2\theta = \frac{2Re\,P_{XY}}{P_{XX} - P_{YY}}\cdot \tag{8}$$

θ is by convention taken positive in the clockwise direction and is referred to as the arrival angle of the H wave.

3. Signal-to-noise ratio (*snr*)

The decoherence (depolarisation) coefficient can be defined in function of the polarisation (coherence) coefficient of the wave as [6]

$$D_D = 1 - P_D, \tag{9}$$

with P_D defined in (5). In the same way as P_D, $0 \leq D_D \leq 1$. By referring to the coherent component as the signal $S(f) = H(f)\cdot P_D$, and the noise $n(f) = H(f)\cdot D_D$, where $H(f)$ is the spectrum of the horizontal magnetic signal. The *snr* can be approximated as

$$snr(f) = \frac{S(f)}{n(f)} = \frac{P_D}{D_D}\cdot \tag{10}$$

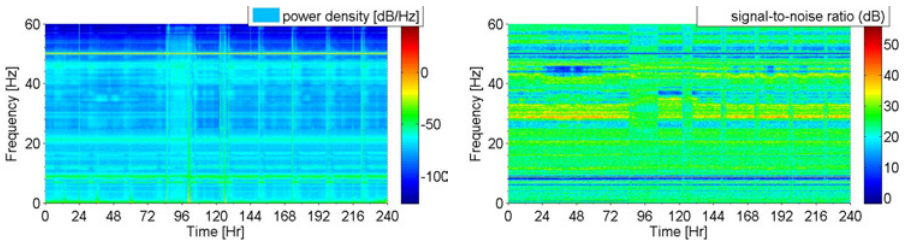

Figure 2. Ten day $[\text{SQUID}]^2$ H power spectral density (left) and *snr* (right graph) starting from 2008-08-22.

Table 1. Peak noise level, average frequency and peak power of the H signal from 2008-08-22 to 31.

frequency (Hz)	6	7.97	50
noise/signal ratio	0.1	0.22	0.32
Peak Power ($\text{pT}^2\text{Hz}^{-1}$)	1	5.4	4×10^5

4. Application to LSBB datasets

Daily geomagnetic datasets sampled at 125 Hz downloaded from the LSBB server[1] are used. The time signal is subdivided in 32.8 s ($N = 4096$) segments which are transformed to the Fourier domain to obtain a spectral resolution of 3×10^{-2} Hz. The spectra are accumulated and averaged over a duration of 24 minutes using Welch's method [7]. For this study, only quiet magnetic datasets are taken into consideration. They are sampled from the minimum solar activity epoch spanning from 2007 to 2009 [5].

4.1 $[\text{SQUID}]^2$ Power density and signal-to-noise ratio spectra

Figure 2 shows H power spectrograms and its *snr* in a frequency range from DC to 60 Hz spanning in time from 2008-08-22 to 31. During the whole period of time, the index of magnetic disturbance is relatively low ($k_p \leq 2$), indicating a worldwide quiet magnetic activity. Maxima in the power of the signal are displayed in Table 1. The *snr* spectrogram in Fig. 2 (right) shows the lowest level at 5 dB at 50 Hz with an average level of noise which is 1/3 of the power in the coherent signal. Table 1 shows the respective peaks of the noise and peak power observed in the spectra.

The peaks of maximum power seem to coincide with the peaks of noise in the spectra as shown in Fig. 2. This might mean that these peaks are caused by an incoherent signal local to the LSBB capsule environment. In an internal report [8], it was shown that switching on the ventilation unit in the capsule caused peaks of noise as high as 30 $\text{pT}/\sqrt{\text{Hz}}$ at 10.3 Hz in all the $[\text{SQUID}]^2$ components.

5. $[\text{SQUID}]^2$ – ICM correlation

ICM polarisation properties are compared to the $[\text{SQUID}]^2$'s in order to demonstrate the presence of a global magnetic signal component at LSBB. Two CARISMA stations distant of 1,200 km in longitude are considered as shown in Table 2. The datasets are sampled on site at 20 Hz thus display only the first SR [9]. The stations are separated from the LSBB by 8,000 km on average.

[1] `http://www.lsbb.eu/index.php/en/`

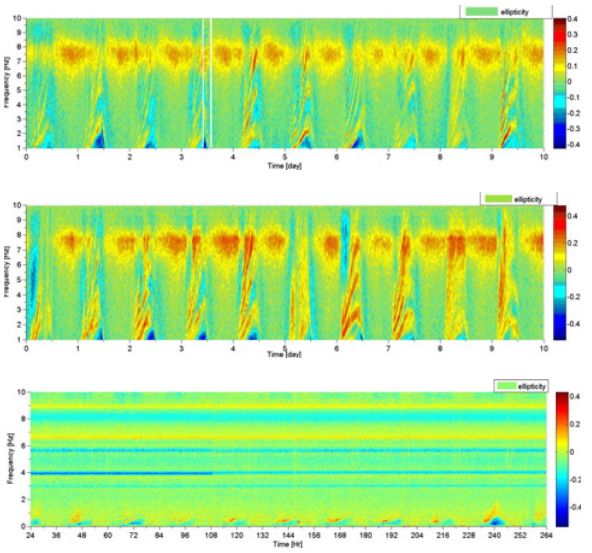

Figure 3. Ellipticity spectrograms from DC – 10 Hz spanning for 10 days from 2008-08-22, at MSTK (top), THRF (middle) and LSBB (bottom).

Table 2. ELF Magnetometer station locations and coordinates.

Site	Location, Country	Lat. North	Long. East
LSBB	Rustrel, France	44.95	87.53
MSTK	Ministik Lake, Canada	53.3	247
THRF	Thief River Falls, USA	57.82	331.49

Figure 3 shows the variation of the ellipticity at the 3 observatories. MSTK and THRF display a maximum (with $el > 0$) band in the vicinity of 8 Hz characteristic of the first SR [6], while at the LSBB the spectra display a minimum ($el < 0$). By considering $|el(f)|$, the spectra at all the stations display a peak at 8 Hz. This indicates that magnetic waves resonate at 8 Hz but are left-hand and right-hand polarised at CARISMA and LSBB respectively (see Sect. 2.2).

The spectra also display local nighttime resonant signals that occur in quiet magnetic conditions that are called ionospheric Alfvén resonances (IAR) [6]. The IAR appear as chirping resonances whose peak frequencies rise in time before they disappear at local-time dawn [6]. In H spectra, the IAR are elliptically polarised and their peak frequencies are highly dependent on the magnetic latitude. For high-latitude magnetic spectra (MSTK and THRF), they can reach frequency ranges up to the first SR (as shown in Fig. 3 top and middle graphs), while for the LSBB signal, the IAR are located in the range of quasi-DC−1 Hz (Fig. 3 bottom graph).

By tracking the extrema of el in the vicinity of 8 Hz, it is possible to determine the variation of the first SR (Δf_0) as a function of time (t). The maximum of the ellipticity at CARISMA station (and the minimum at LSBB) and their corresponding peak frequency are recorded in the spectra for every 12-minute. The resulting signals $el(t)$ and $\Delta f_0(t)$ are Fourier transformed, yielding $el(f)$ and $\Delta f_0(f)$ with a cutoff frequency of 60 day^{-1}. $el(f)$ and $\Delta f_0(f)$ display harmonics embedded in the time-dependent signals as shown in Fig. 4 (left). In order to study diurnal variations, the signals are filtered through a passband filter centered at the first daily harmonic ($f = 1$ day^{-1}) with respect to the bandwidth in their spectra. Figure 4 (right) shows the diurnal variations of el and Δf_0.

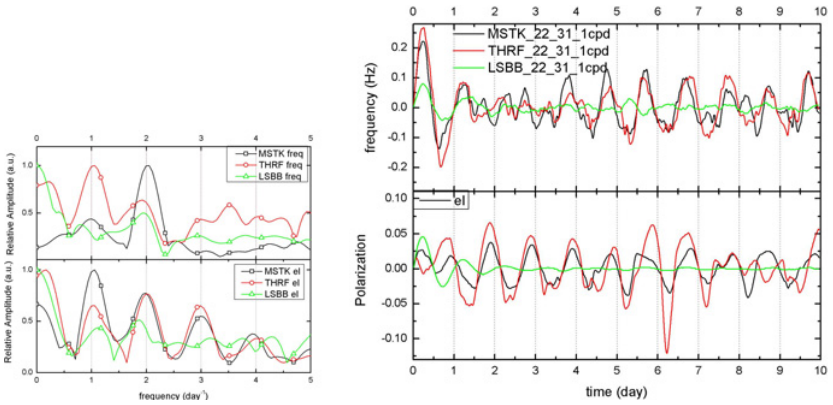

Figure 4. Diurnal variation of the frequency (top graph) and ellipticity (bottom graph) during the quiet magnetic period 2008-08-22 to 31. The spectra [left side] and the filtered signals around 1 day^{-1} [right side] are represented.

As depicted in Fig. 4, CARISMA stations show a diurnal variation in time of the ellipticity comparable to [2] and peak frequency diurnal variation that is similar to the first SR [10]. The diurnal *el* and Δf_0 variations at CARISMA stations are highly correlated. Frequency and polarisation variations at LSBB are not correlated with those at CARISMA stations and the peak ellipticity in the vicinity of 8 Hz is constant throughout the whole dataset.

6. Conclusion and recommendations

The coherence matrix has proven to be a straightforward and stable method to evaluate the degree of polarisation of geomagnetic signals at the LSBB. In the lower ELF range (1−60 Hz), the signals that are coherent can be associated with a global resonance and those uncoherent discarded as localised noise. The latter are observed at 6, 7.9 and 50 Hz in the *snr* spectra. $[\text{SQUID}]^2$ *H* spectra do not clearly display the first SR because the amplitude of variation of the ellipticity and peak frequency are much lower than those observed in the ICM data. Therefore, *H* polarisation properties of another (SQUID) magnetometer local to the LSBB, but not located in the capsule, should be evaluated as a comparison to the $[\text{SQUID}]^2$'s.

The author thanks I.R. Mann, D.K. Milling and the rest of the CARISMA team for data. He is also thankful to the LSBB team and their collaborators for providing the $[\text{SQUID}]^2$ data.

References

[1] Nickolaenko A. P., Hayakawa M., *Resonances in the E-I Cavity* (Springer Sc., Tokyo, 2002).
[2] Sentman D.D., Radio Sci. **22**, 595–606 (1987).
[3] Born M. & Wolf E., *Principles of Optics* (Mac-Millan, New York, 1959).
[4] Fowler R.A., Kotick B.J. & Elliott R.D., Geophys. Res., **72**, 2871–2883 (1967).
[5] Kwisanga C., *SQUID Geomagnetic Signal Analysis and Modelling of SR in the E-I Cavity* (E & E Eng., Stellenbosch, 2016).

[6] Nickolaenko A.P. & Hayakawa M., *Schumann Resonances for Tyros* (Springer, Tokyo, 2014).
[7] Welch P.D., IEEE Trans. Audio & Electroac., **15**, 70–73 (1967).
[8] Bernard S., Pozzo di Borgo E., & Febvre P., LSBB Tech. Rep. 27–28 July (2010).
[9] Mann I.R., *et al*., Space Sci. Rev., **141**, 413–451 (2008).
[10] Price C. & Melnikov A., Atmos. Sol.-Terr. Phys., **66**, 1179–1185 (2004).